Direct synthesis of hydrogen peroxide at additively manufactured fluid guiding elements as structured catalysts[☆]

Laura L. Trinkies [a,*], Derrick Ng [b], Zongli Xie [b], Christian H. Hornung [b], Manfred Kraut [a], Roland Dittmeyer [a]

[a] Institute for Micro Process Engineering - Karlsruhe Institute of Technology, Hermann-von-Helmholtz-Platz, 1, Eggenstein-Leopoldshafen 76344, Germany
[b] CSIRO Manufacturing, Bag 10, Clayton South 3169, Victoria, Australia

A B S T R A C T

To facilitate the change from a centralized to a decentralized production of H_2O_2 whilst increasing the overall safety of the production, the direct synthesis of H_2O_2 is currently being investigated as an interesting alternative to the established anthraquinone auto-oxidation process. However, for this approach a reliable and industrially viable solution is needed to immobilise the catalyst inside the reactor system, thus eliminating the need for cost and time intensive post process removal of the catalyst from the product as it is practiced in current existing slurry reactors. In this work we present a route to coat Pd/TiO_2 catalyst onto additively manufactured steel substrates via a simple washcoating process. The resulting structured catalysts show good activity towards the direct synthesis reaction and can be considered stable for the herein investigated process, since they do not show any deactivation during repeated measurements, nor was any mass loss of the coating observed. The sustained catalyst performance and the uniform physical properties of the coatings are attributes of the reliability and reproducibility of the coating process.

1. Introduction

Hydrogen peroxide (H_2O_2) is increasingly gaining importance as a so called green oxidizing agent [1,2]. Its potential to chloridic oxidiziers has been recognised by many sectors such as paper and pulp industry [3–5], waste water treatment and clinical disinfection [3,6]. However, the current main production route via the anthraquinone auto-oxidation process [7] is still preferably used for the production on a larger scale (> 40,000 t a^{-1} [8]), because of the high energy demand of the synthesis process [3] and the subsequent waste processing [9]. Thus, up to now, H_2O_2 is mainly produced in centralised mega-plants [8,10], which makes it necessary to transport H_2O_2 to the end-user, often over large distances [11]. To maintain the productions economic feasibility, the product is often concentrated before its transport, to reduce the transport costs per gram H_2O_2. But, since most end-user applications require lower concentrations of H_2O_2, the chemical has to be re-diluted again at its final destination. The additional intermediate concentration, the transport itself and the final re-dilution step not only increase the cost of H_2O_2 [3], but also lead to a non-negligible safety risk during the transport, as the concentrated H_2O_2 is highly explosive [11,12].

For this reason, a lot of research has been conducted to explore alternative, decentralised production ways for H_2O_2 over the past decades [11]. The direct synthesis over noble metal catalysts in a liquid phase presents an alternative of interest. Supported noble metal catalysts as palladium or platinum have proven to be very active for this reaction [8]. However, noble metal catalysts not only enhance the H_2O_2 synthesis reaction itself ($H_2 + O_2 \rightarrow H_2O_2$), but also catalyse the undesired side reactions including water formation ($H_2 + \frac{1}{2}O_2 \rightarrow H_2O$), the consecutive decomposition of H_2O_2 ($H_2O_2 \rightarrow H_2O + \frac{1}{2} O_2$) and the hydrogenation reaction ($H_2O_2 + H_2 \rightarrow 2 H_2O$). Therefore, development and tuning of the catalyst system is highly desired and of great interest for current research [13–16].

But not only a suitable catalyst system is needed to flatten the path in the direction of a decentralised production, also an innovative reactor concept has to be found to deal with the challenges arising from the direct combination of H_2 and O_2. Inoue et al. developed a microstructured lab scale reactor with channel width and depth of 600 μm and 900 μm respectively to improve the mass transfer in the system and at the same time keep the dimensions of the reactor channels below the ignition length of H_2/O_2-explosions. In this concept the catalyst is implemented as a fixed-bed [17]. Fixed-bed reactors, however, are often

associated with diffusion limitations, limiting the overall efficiency of the reaction system [18]. Selinsek et al. made progress on the design of a microstructured membrane reactor with incorporated reactant resaturation. By introducing a membrane into the concept, the bubble-free dosage of the reactants is made possible [19,20]. In this reactor system, the catalyst needs to be suspended in the liquid reaction medium or be applied as a wall coating [20]. This means, the catalyst has to be separated from the product solution after the reaction or the whole reactor has to be serviced to recover the catalyst after the process respectively.

Continuous flow processes are already commonly used in the chemical industry (i.e. [21]), but are gaining increasing importance also in the pharmaceutical industry [22]. Supported structured catalysts have the capability to contribute to the sustainable chemical industry of the future [23]. Flow enhancing structures as static mixers [24–26] or fluid guiding elements (FGE) [27,28] are possible channel inserts which not only enhance mass transfer processes in the reacting fluid, but can serve as catalyst carriers at the same time, replacing conventional wall-coatings. In comparison to conventional fixed-beds, they reduce the observed pressure loss and lead to less temperature hot-spots in the reactor system [26].

In this work we present a simple and scalable catalyst coating method onto a specifically additive manufactured structured catalyst support for the direct synthesis of H_2O_2 while maintaining considerable activity and stability for the use in an envisioned tubular membrane reactor. The additive manufactured fluid guiding elements (FGE) [27], were chosen as flow enhancing geometry for the catalyst substrate structure. The main benefit of this form of process intensifying channel inserts is the enhancement of mass transfer in combination with the preservation of a low pressure drop resulting from the laminar flow regime, as confirmed by different simulations [27,29]. The catalyst of interest is a Pd/TiO_2, as compared with a commercial Pd/Al_2O_3 catalyst. Thoroughly investigated by density functional theory (DFT) calculations and experiment, Pd shows the most promising catalytic activity towards the direct synthesis of H_2O_2 amongst the monometallic catalysts in question [8,30]. The easy adaptability and scalability to variate catalyst systems [31] makes washcoating processes attractive for industrial applications. For these reasons, a washcoating procedure is chosen to apply the catalyst on the channel inserts. The productivity of the developed coatings is used to quantify and compare the suitability of the coatings for the direct synthesis application, with respect to the chosen catalyst support, i.e. Al_2O_3 and TiO_2, and Pd-loading, i.e. 1 wt.-% and 5 wt.-% and investigate possible catalyst deactivation. Optical inspections and element analysis of catalyst coating after the reaction are conducted to study the stability of the coatings. The reproducibility, and therefore reliability of the coating procedure, is assessed via the determination of the deposited amount of catalyst and the productivities achieved with different samples.

2. Methods

2.1. Design and fabrication of the carrier structures

Specially designed and additive manufactured FGE are used as carrier structures and catalyst substrate for the supported catalysts. One FGE consists of several radially and axially aligned fluid guiding blades (FGB) and plane intermediate segments (ISE), which together can be summarised as a fluid guiding unit (FGU). Several FGUs are arranged in radial and axial direction to form the final fluid guiding element. The general working principle of the geometries was first presented in [27]. The segment of an FGU from FGBs and ISEs is shown in Fig. 1a and b in top and isometric view respectively.

These complex structures cant be fabricated by classic manufacturing methods which is why they are formed from metal powder by a powder bed fusion process of metals using a laser-based system (PBF-LB/M).

The design of the structures is created in Autodesk Inventor® and exported to IGS-file format using the internal export. The IGS-files are afterwards converted to readable STL-files using PTC Creo® to ensure better compatibility. The samples are then manufactured on a Realizer SLM 125 (DMG Mori, Germany) machine. The system is equipped with a 400 W yttrium fibre laser and a F-Θ lense system. The squared building plate has a size of $125 \times 125mm^2$ and therefore offers the option to print
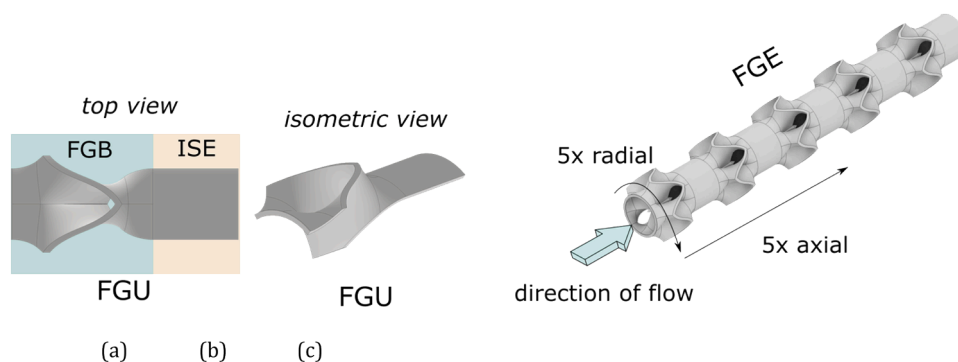
Fig. 1. Schematic representation of a FGU consisting of FGB and ISE segments in top and isometric view, (a). Illustration of a FGE with five radial and axial FGUs, respectively, the flow direction is indicated by a green arrow, (b).
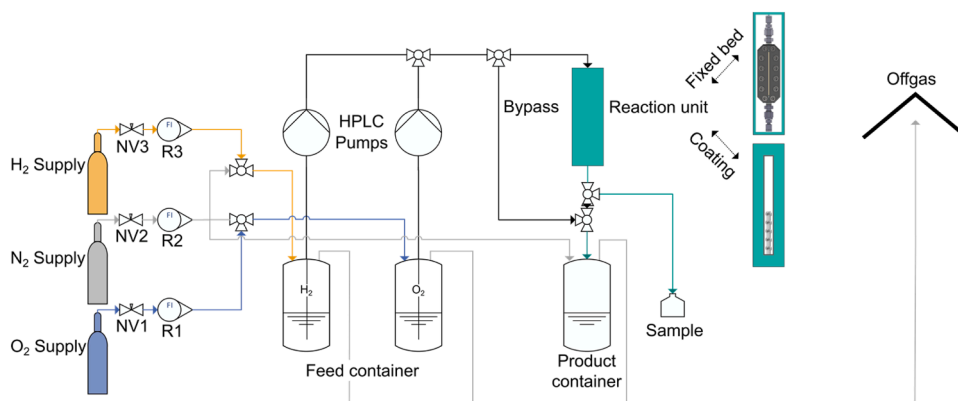
Fig. 2. Process flow diagram visualizing the experimental set-up for the conducted measurements to investigate the activity of the coatings.

several specimens at once. To print the structures, a spot size of around 25 μm is chosen to melt the stainless steel powder (1.4404, Carpenter Additive, UK ($d_{3,50}$ = approx. 31 mm)). For this study, structures with five axial and five radial FGUs are used as carriers for the catalyst. The resulting FGE geometry is given in Fig. 1c.

2.2. Catalyst preparation

In our case, a Pd/TiO$_2$ catalyst with different Pd-loadings, i.e. 1 wt.-% and 5 wt.-% Pd, was synthesised via an adapted incipient wetness impregnation procedure [32,33], as described in [34].

Briefly, palladium(II) nitrate hydrate (Pd(NO$_3$)$_2$xH$_2$O, ACROS Organics) and titania (BET-surface area: 35-65 m^2 g^{-1}, AEROXIDE® TiO$_2$ P25, Evonik Industries) are each dispersed under continuous stirring in deionized water (DI, MilliQ) at 80 °C. The palladium nitrate solution is then slowly dripped into the homogeneous titania suspension under continuous stirring at 80 °C using a single-use syringe. The suspension is kept at 80 °C and further stirred, until its texture becomes paste-like. This paste is dried under static air at 110 °C (ramp of 5 °C min^{-1}) for 11 hours in a muffle furnace (M110, Thermo Scientific) to remove water residues, followed by calcination at a set temperature of 400 °C (ramp of 9.7 °C min^{-1} from 110 °C for 5 hours) for further 3 hours in the same furnace. To shatter possible agglomerates, the catalyst is mortared by hand and sieved into fractions below 200 μm (Analysette 3 PRO sieving machine, Fritsch GmbH). The palladium on the catalyst is then activated in a final reduction step, by heating it to 200 °C in a 5 % H$_2$ in Ar flow (Arcal15, AirLiquide) for 3 hours (ramp of 2.8 °C min^{-1}) in a tube furnace (RO 4/25, Heraeus). The catalyst is then sieved into fractions of

surface, which requires the preparation of a catalyst slurry. In our study the sieved fraction of below 50 μm is derived from the catalyst described in 2.2 dispersed into water to form the coating slurry for the subsequent washcoating steps. Stainless steel is known to decompose H$_2$O$_2$. For this reason, prior to coating, the FGEs are passivated in a bath of nitric acid, following the passivation procedure, as described in [35]. The FGE are then rinsed thoroughly with water afterwards.

The catalyst deposition was achieved via an easily scalable washcoating procedure [25]. First, a washcoating slurry typically containing 15 wt.-% of solids was prepared by adding the respective catalyst powder to deionized water and stirred for several hours to form a homogeneous slurry mixture. The pre-treated stainless steel FGEs were oven dried at 110 °C for 2hours before washcoating them by dipping them into the catalyst slurry for a few seconds followed by removal of the excess material to prevent blockage of the internal openings of the FGEs. The washcoated FGEs were dried at room temperature for over 16 h and subsequently in a fan forced oven at 120 °C for a further 4 hours. The washcoating and drying steps were repeated several times until the desired catalyst loading value (typically 9.2–9.8 wt.-% of 1 wt.-% Pd/TiO$_2$ catalyst) was achieved. The amount of catalyst loading is determined via weighing of the FGE samples before the first coating cycle (blank specimen) and at the completion of the whole coating process. In order to clearly categorise our synthesis experiments it was decided to use a nomenclature; the simple coding in (1) below gives a brief explanation of the used identifiers including an example of the first experimental run with washcoated sample *A* with a layer of 5 wt.-% Pd/TiO$_2$. The first part of the coding described the form of the investigated catalyst, washcoat (= WC) or fixed bed (= FB). The identifiers for the support material, i.e. Al$_2$O$_3$ and TiO$_2$, are represented by

$$\underbrace{\text{WC}}_{\substack{\text{washcoating} \,|\, \text{fixed bed}}} - \underbrace{\text{01}}_{\text{Al}_2\text{O}_3 \,|\, \text{TiO}_2} - \underbrace{5}_{\text{wt.−\% Pd}} - \underbrace{\text{A}}_{\substack{\text{specimen identifier} \\ \text{(optional)}}} - \underbrace{\text{I}}_{\substack{\text{no. of experiment} \\ \text{(optional)}}} \qquad (1)$$

50–200 μm and below 50 μm. The particle sizes are confirmed by static laser light scattering measurements (HORIBA LA-950, Retsch Technology) of 1 g of dispersed catalyst particles in ethanol.

A commercial 5 wt.-% Pd/Al$_2$O$_3$ catalyst (Sigma-Aldrich) was used for the comparative investigations of the support.

2.3. Catalyst coating

Washcoating procedure is used to depositing catalysts onto metal

a digital descriptor (1 = yes, 0 = no).

Table A.2 in the Appendix gives a detailed overview over the samples.

2.4. Reaction assessment

2.4.1. Test rig

Fig. 2 shows a schematic of the test rig used to examine the reactive behaviour of the structured catalyst. Its configuration is adapted from

[36]. It enables the dosage of a bubble-free reaction mixture which makes it possible to study equimolar H_2/O_2 ratios without the necessity to dilute the composition with an inert gas. Though this configuration leads to a limitation of gaseous reactants due to the saturation limit of the liquid phase, this setup is deemed suitable for our proof-of-concept study presented hereafter. Two feed container filled with the solvent are presaturated with hydrogen and oxygen via rotameters. Both containers as well as the product container can also be flushed with nitrogen for safety reasons. Two high performance liquid chromatography (HPLC) pumps (BlueShadow 40P, Knauer) control the flow of the presaturated solvents. Before entering the reaction unit, the two single phase liquid streams are mixed in a tee piece. The depicted bypass can be used to confirm the presence of a bubble-free flow, as required by safety precautions. A sampling tap is installed directly after the reactor to pour samples for external UV–vis analysis (see Section2.4.2) of the product containing solution. The tubing between the feed containers and the sampling tap are all made of stainless steel. To investigate the coated structures, the specimen is inserted into a 10 mm stainless steel tube with the long ISE pointing downstream. Before each experiment, the correct orientation of the sample in the test tube is ensured. The tube was then mounted in the position of the reaction unit, as indicated in Fig. 2.

For the fixed bed experiment, 16 mg of the solid catalyst powder (fraction: 50 - 200 μm) are loaded in the cuboid slit of a stainless steel microreactor flow cell. A more detailed description of the design of the flow cell can be found in [36]. Before and after the catalyst bed, a layer of quartz wool, silicon carbide (sieve fraction: 50–200 μm, Alfa Aesar) and another layer of quartz wool were filled into the reactor to compact the bed and prevent the catalyst from being washed out. The filled flow cell was then mounted in the position of the reaction unit, as indicated in Fig. 2.

2.4.2. H_2O_2-quantification via UV–vis spectroscopy

UV–vis spectroscopy is a commonly used photometric method to determine the concentration of H_2O_2 in solutions. Its concentration can be derived from the absorbence of the yellow-coloured complex, which H_2O_2 forms with titanium(IV) oxysulfate [37]. The measured absorbence can be directly converted into the concentration of H_2O_2 according to a calibration using known H_2O_2 concentrations.

The aqueous titanium reagent is prepared according to the method described in [38]: 25 g of $TiOSO_4$ (pro Analysis, Riedel-de Haen®) are added to 1 L of $2 mol\ L^{-1}$ sulfuric acid (95–97 % for analysis, Sigma Aldrich) under continuous stirring.

For the measurements, the product sample containing H_2O_2 is mixed with the titanium sulfate solution with a ratio of 9:1. The sample mixture is analysed in a 5 mm optical quartz glass cuvette (QS, Hellma Analytics) using an Agilent 8453 UV–vis spectrometer at 409 nm wavelength. Each product sample mixture is analysed five times to minimise measurement uncertainties. To avoid systematic measurements errors, the samples are analysed in randomized order.

2.4.3. Experimental proceeding

The described test rig mainly consists of stainless steel tubing, which, as already mentioned in Section2.3, is known to decompose H_2O_2. All metal parts are thus also passivated following the standard passivation procedure using nitric acid prior to use [35].

Before each experimental run, gaseous H_2 and O_2 are bubbled into the aqueous reaction medium (H_2O (DI, MilliQ) + 0.15 mmol L^{-1} H_2SO_4 (95–98 %, Sigma Aldrich) + 4mmol L^{-1} NaBr (Merck)) for two hours. The reaction medium is stored in two separate feed containers. This procedure ensures that each feed is fully saturated with the respective gas. Afterwards, hydrogen saturated solvent (flow rate: $\dot{V}_L$ =5 mL min^{-1}) is led over the investigated catalyst for 30minutes to create standardised metal oxidation conditions of the catalyst in each experimental run. After the 30minutes, H_2 -and O_2-saturated solvent (total

flow rate: $\dot{V}_L$ =5 mL min^{-1}) is led through the reaction unit for the synthesis reaction experiments. 50 mL of the resulting product containing solution are collected in clean glass bottles and are stored cool and dark until analysis via UV–vis spectroscopy. The stability of the samples has been verified vicariously for randomly chosen samples by repeated analysis of the same sample at random points of time over the course of up to eight weeks.

To investigate the hydrogenation behaviour of the coating, 1 mM H_2O_2 solution in aqueous reaction medium is flushed with nitrogen for two hours in one of the feed vessels, to ensure that no oxygen is present in the solution. Gaseous H_2 is bubbled into the pure reaction medium in the other container at the same time. Also, in these experiments, the investigated catalyst is hydrogenated by exposing it to the hydrogen saturated solvent for 30minutes. The feed is switched again and hydrogen saturated reaction medium as well as H_2O_2-spiked solvent are led through the reactor with a total flow rate of $\dot{V}_L$ =5 mL min^{-1}, while ensuring an equimolar mixing ratio of 1:1. For each experimental run, the spiked solution is analysed for its exact H_2O_2concentration prior to the experiment. The decomposition activity of the catalyst is checked in another set of experiments, in which only 1 mM H_2O_2 spiked solvent is led through the reaction unit. Again, the spiked solvent is flushed with nitrogen and each coating is activated by exposure to hydrogen saturated pure solvent prior to each experiment for 30minutes. The H_2O_2concentration of the feed before the reaction is monitored, as well. After the activation of the catalyst, the feed stream is changed to the H_2O_2 spiked solvent stream (flow rate: $\dot{V}_L$ =5 mL min^{-1}).

All experiments are conducted under ambient pressure and at room temperature.

2.4.4. Productivity assessment

The productivity of the catalyst towards the synthesis of H_2O_2 is chosen as a measure to evaluate the suitability of the proposed coatings. The catalyst effectiveness is assessed by the H_2O_2 formation rate expressed as mol of H_2O_2 and liquid volume flow rate per unit mass of metal catalyst in Eq. (2). To compensate for operational instabilities and measurement deviations, the mean productivity is determined. Therefore, the productivities of each sampling time are summed up to their weighed mean, using the standard deviation as a weighing factor. The synthesis reaction is performed in the test rig described in 2.4.1.

$$productivity_{synthesis} = \frac{c_{H_2O_2} \cdot \dot{V}_L}{m_{Pd}} \qquad (2)$$

The productivity of the catalyst for the hydrogenation reaction is assessed accordingly after the relation formulated in Eq. (3).

$$productivity_{hydrogenation} = \frac{\left(c_{H_2O_2,\ in} - c_{H_2O_2,\ out}\right) \cdot \dot{V}_L}{m_{Pd}} \qquad (3)$$

To precisely describe the productivity, it is necessary to identify the exact amount of the active metal component in the catalyst (layer). Therefore, inductively coupled plasma optical emission spectrometry (ICP-OES) measurements are performed on the fresh catalyst using an iCAP 7600 Duo from Thermo Fisher Scientific.

2.4.5. Stability assessment

To assess the stability of the catalytic coating after each run, the same wash coated sample is tested under reaction conditions for several times. The sample specimen is demounted from the reactor tube after 7 h on stream and is air-dried under ambient conditions over night. The productivities are then compared over the course of 7 h.

In order to qualitatively identify possible leaching and grade the adhesion of the catalyst, the examined samples are weighed with a high precision balance (ABJ-M/ABS-N, Kern®) before and after each experimental run.

The composition of the coating after the reaction can serve as an indicator for possible corrosion processes. Again, ICP-OES analyses are
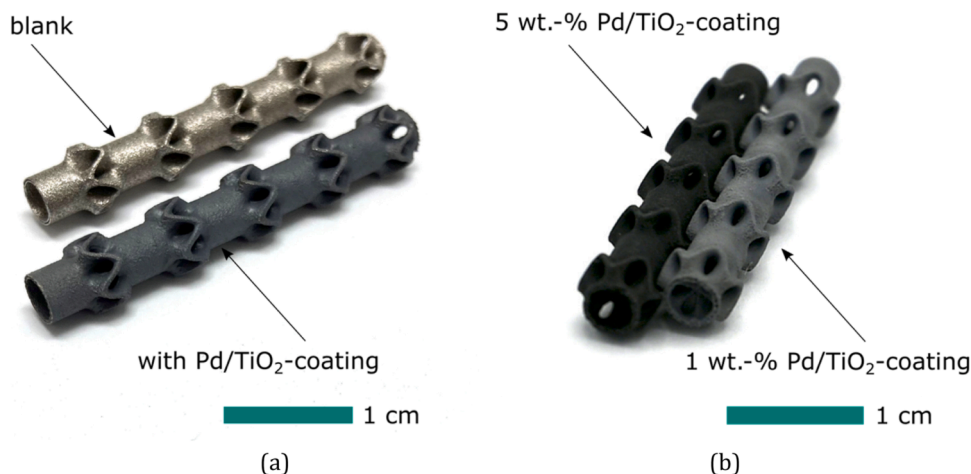
Fig. 3. Picture of the prepared coated structures: before (blank) and after coating (1 wt.-% Pd/TiO$_2$). The applied 1 wt.-% Pd/TiO$_2$-coating is clearly identifiable by the black colour (a). Picture of the samples with different Pd-loading, i.e. 5 wt.-% Pd/TiO$_2$ and 1 wt.-% Pd/TiO$_2$ (b). The higher metal content leads to an almost black appearance of the coating after the final reduction step.
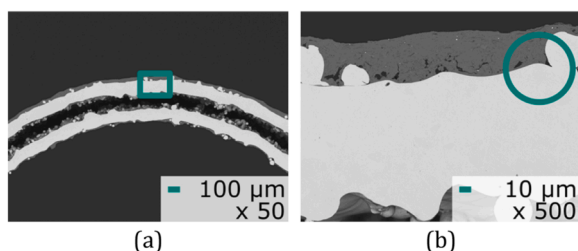
Fig. 4. SEM images of the cross section of a coated FGE at the position of an ISE. Magnification of 50 (a) and 500 (b).

conducted. For the preparation, around 100 mg of the coating are scraped off the surface of the support structure and decomposed by acid using temperature and pressure.

2.4.6. Reproducibility

The reproducibility of the coating method is quantified by coating two carrier structures following the same procedure. For both runs the amount of deposited catalyst is determined via weighing of the samples as indicated in 2.3.

The samples are then consecutively exposed to reaction conditions and the productivities measured over seven hours on stream are compared.

3. Results and discussion

3.1. Evaluation of the coating

Fig. 3a shows a picture of the uncoated FGE substrate and the FGE substrate after the application of the washcoating, respectively. The applied coating appears as a uniform layer and the geometric details of the FGE are preserved. Since the openings of the different blades are not blocked by the application of the coating, the flow guiding function of the substrates is sustained.

SEM images of the coating. In Fig. 4 the cross-section of the coated
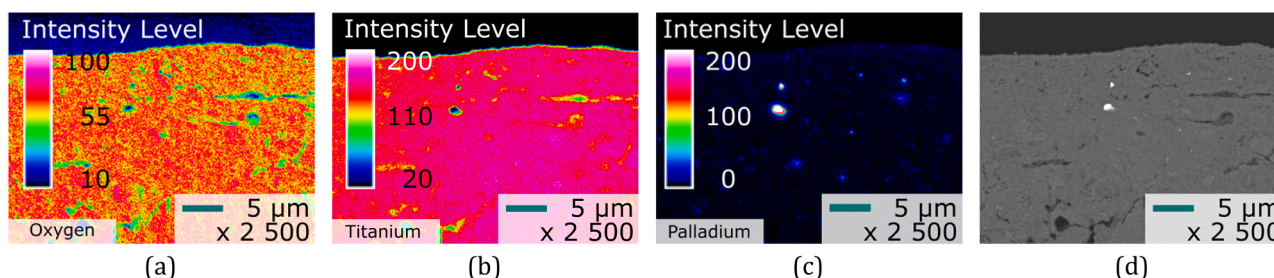
Fig. 5. Maps of the element distribution from WDX-measurements with magnification factor of 2500: material content for O$_2$ (a), Ti (b) and Pd (c) as well as the corresponding SEM-image as a reference of the 1 wt.-% Pd/TiO$_2$-coating applied as washcoating in this work (d).
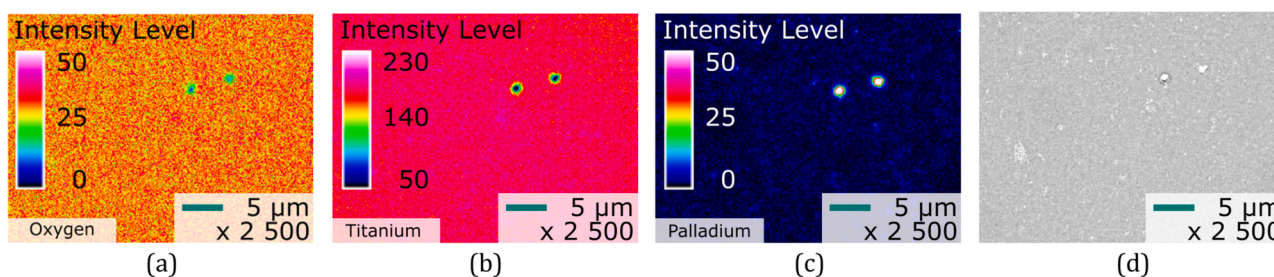
Fig. 6. Maps of the element distribution from WDX-measurements with magnification factor of 2500: material content for O$_2$ (a), Ti (b) and Pd (c) as well as the corresponding SEM-image as a reference of the 50–200 μm fraction of the 1 wt.-% Pd/TiO$_2$ catalyst used as catalyst for the washcoatings in this work (d).

(a) Total synthesis reaction

(b) Total synthesis reaction

(c) Decomposition of H_2O_2

(d) Hydrogenation of H_2O_2
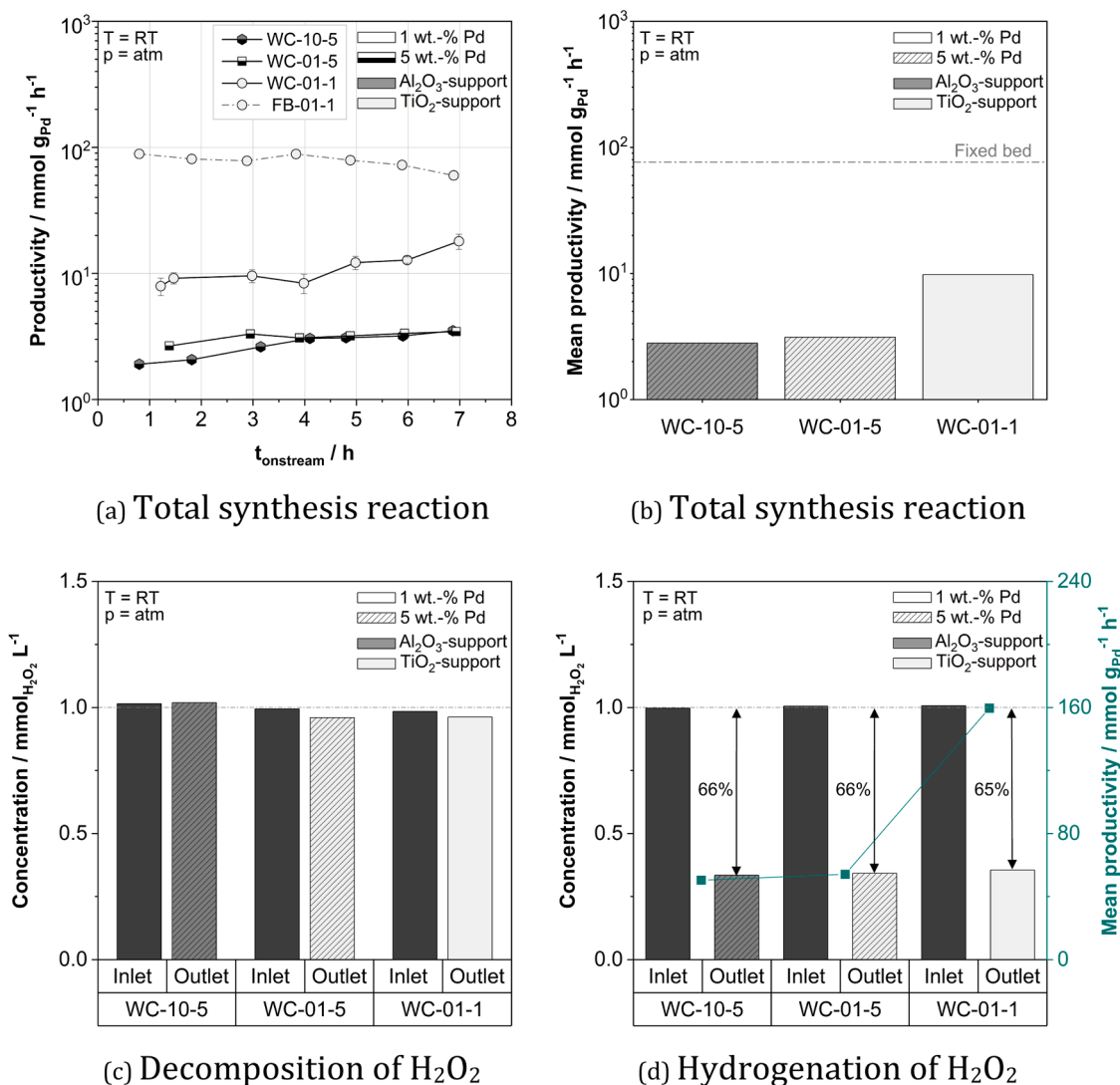
Fig. 7. Comparison of the synthesis activity of the investigated catalyst coatings with different support materials and Pd-loadings, expressed as productivity over time on stream (a), the synthesis activity of the investigated catalyst expressed as mean productivity (b), the measured concentrations at the inlet and outlet of the reactor for the decomposition of H_2O_2 (c) and the observed concentrations as well as the resulting productivities for the hydrogenation of H_2O_2 (d). Lines between the measurement points do not represent measured data and are added to guide the eye.

sample is shown in images from scanning electron microscopy (SEM) (JXA 8530F, JOEL) with different magnifications, the green rectangle in Fig. 4a marking the image detail magnified in Fig. 4b. From the scale bars, an active layer thickness of approximately 100 μm can be calculated. The white spots visible in the dark-grey layer are the Pd dispersed in the TiO$_2$. The dark patches are hollow areas, the pores. It can also be seen that the layer does not perfectly cover the indentations, as marked by the green circle in Fig. 4b. These undercuts are stemming from molten metal powder particles from the manufacturing process of the substrate. It can also be seen that the wall of the substrate itself does not contain any molten material, but is hollow. This is due to the chosen laser scanning strategy in the additive manufacturing process.

WDX of the coating. Wavelength-dispersive x-ray spectroscopy (WDX) (JXA 8530F, JOEL) of the coating exposes an even distribution of the active component in the layer, as the maps in Fig. 5 are showing. Pores in the layer can be identified by dark colours, specifying the absence of the respective species (Fig. 5a-c). Unfortunately, adsorption measurements using BET analysis (Gemini VII, Micromeritics) wasn't able to quantify the porosity of the coated surface, because of the large amount of the FGE scaffold.

WDX of the catalyst. Maps of the elements O$_2$, TiO$_2$ and Pd have been

conducted by WDX measurements to closely investigate the distribution of the elements in a 1 wt.-% Pd/TiO$_2$ catalyst. As it can be seen in Fig. 6c, the Pd is mostly evenly distributed in the TiO$_2$ matrix, with the exception of two larger agglomerates that were captured within this image, Fig. 6a and b. ICP-OES analyses of this powder catalyst confirmed the targeted loading of 1 wt.-% Pd, see distributions in the Appendix.

3.2. Productivity

Fig. 7 shows the measured productivities for the overall synthesis reaction, the concentrations measured in the experiments for the decomposition of H_2O_2 and the concentrations as well as accordingly calculated productivities for the experiments of the hydrogenation of H_2O_2 for the different samples. The activity towards the synthesis reaction for the samples WC-10–5 and WC-01–5 with identical, i.e. 5 wt.-% Pd-loading on two different support materials, i.e. Al$_2$O$_3$ and TiO$_2$, does not vary significantly over the course of the experiments, as can be seen in Fig. 7a. The visible variations within each sample are most likely traces resulting from instabilities in the operational conditions of the setup, such as a slight oversaturation of the feed with one of the reactant gases due to fluctuations in the dosage system. The increase of the
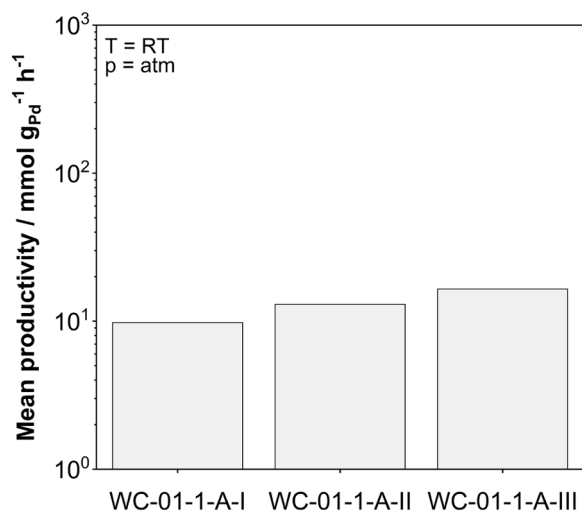
Fig. 8. Qualitative assessment of the catalytic deactivation of the coating by the comparison of the mean productivity of one specimen for several runs after drying over night. Due to the scaling of the plot the corresponding error bars are not visible.

Table 1
Masses of the blank support structure (m_{blank}), net mass of Pd/TiO$_2$ catalyst loaded onto the support structure after washcoating ($m_{cat, net}$) and deducted catalyst loading (load$_{cat}$).

Sample	m_{blank}	$m_{cat,net}$	load$_{cat}$
–	g	g	%
Batch 1	1.3923	0.123	9.31
Batch 2	1.4323	0.126	9.27

measured concentrations over time, and hence increasing productivities, is in good agreement with observations in recent studies by Brehm et al. [39].

The derived mean productivities, which were derived in order to make experimental sets comparable by correcting for operational conditions, do confirm the described trend, as indicated in Fig. 7b. A slightly higher synthesis productivity is observed for the coatings on TiO$_2$-supports. For some experimental sets the calculated standard deviations are neglectable. In order to evaluate the selectivity of the coatings qualitatively, separate measurements looking at the H$_2$O$_2$-decomposition

activity and the H$_2$O$_2$-hydrogenation activity have been conducted. The activity of the evaluated coatings with respect to the investigated support material towards the decomposition reaction can be neglected for both support types, as can be seen in Fig. 7c. A difference of less than 4 % between the measured inlet and post-reaction concentration of H$_2$O$_2$ in the solvent is observed. The corresponding measurements evaluating the hydrogenation reaction show comparable activities of the catalyst across all samples for this reaction. For both support types a reduction of 66 % of the inlet H$_2$O$_2$-concentration is measured, see Fig. 7d. A finite conclusion about the impact of the support material on the subsequent reaction paths can not be drawn. However, under our reaction conditions, the impact of the support materials investigated in this study, i.e. Al$_2$O$_3$ and TiO$_2$, on the activity of the catalyst towards the decomposition reaction of H$_2$O$_2$ and one towards the hydrogenation of H$_2$O$_2$ appears to be negligible. The impact of the metal component loading on suspended catalysts for the direct synthesis of H$_2$O$_2$ is subject of several studies in literature [39–41]. Thus, this aspect is also deemed important for the evaluation of the coatings present in this work; here we looked at different Pd loadings on TiO$_2$. Although stronger fluctuations in the determined productivity for the direct synthesis reaction over time can be observed for the 1 wt.-% Pd/TiO$_2$ coated substrate than for the other specimen, it is still very clear to see that the measured productivities, related to the amount of Pd in the system, exceed the ones achieved with the 5 wt.-% Pd/TiO$_2$ sample, Fig. 7a. A slight increase in the productivity with time is observed for the different samples and might be attributed to a change in the hydrogenation state of the catalyst. The fluctuations in the time dependent outline are again attributed to fluctuations in the system environment. Since there is substantially less catalyst, the amplitude is increased. Nevertheless, the described overall trend becomes even more apparent in the comparison of the respective mean productivities, Fig. 7b and is in general in good agreement with findings from literature [40,41], suggesting an increase of the selectivity with a decrease in Pd-loading. As can been taken from Fig. 7c, the decomposition activity of the two coatings with different Pd-loadings is low and almost equal. Also, the activity, expressed as difference in the measured concentration at the inlet and outlet, for the hydrogenation of H$_2$O$_2$ seems to be comparable for both loadings. However, the calculated productivities scaled with the respective Pd-loading do show a higher activity of the catalyst with the lower metal loading.

The grey markers connected by the dotted line in Fig. 7a represent the temporal evolution of the H$_2$O$_2$ productivity for the 1 wt.-% Pd/TiO$_2$ catalyst synthesised according to the procedure described in 2.2 investigated as a fixed bed. As it can be seen, no apparent run-in time can be observed. The productivity decrease might be explained by the lower
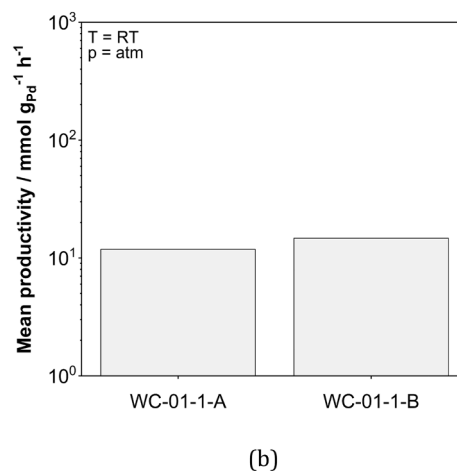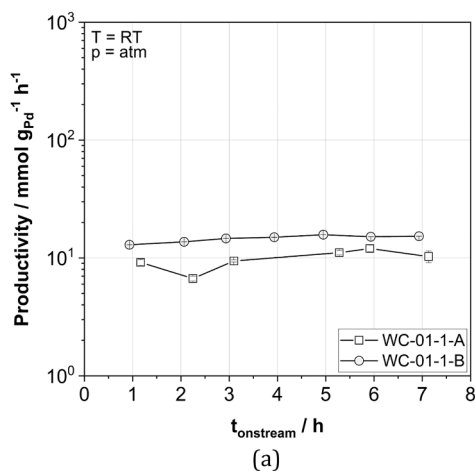
Fig. 9. Reproducibility of the washcoating procedure accessed by the mean productivity of specimens from two different coating batches. Productivity over time (a) and mean productivity (b).

accessibility of the active sites of the Pd in the coating. Reasons for this could be the low porosity of the coated layer. Another possible explanation might be that less of the active sites for the synthesis reaction, such as (111) faces [42], are accessible in the coating. However, after around four hours, a slight decrease in the productivity of the catalyst in the fixed bed appears, a clear disadvantage in comparison to the structured catalysts used.

3.3. Stability

Interruptions of the envisioned industrial process are possible, i.e. for service and maintenance reasons or black-outs. Thus, deactivation of the catalyst after a period of dry-out has to be precluded and is investigated. In general, H_2O_2 and sulphuric acid are known to enhance the corrosion of metal surfaces [43,44]. To assess the susceptibility of the coatings towards this form of ageing, optical inspections of the catalytic coatings and element analysis via ICP-OES of the coatings after the exposure to the reaction medium are conducted. Also, the samples are weighed before and after each experimental run to quantify the amount of leached catalyst.

3.3.1. Productivity

The derived mean productivities for the same sample after three runs show no apparent loss in the catalytic activity of the coating, as can be seen in Fig. 8. On the contrary, the productivities observed seem to increase with each test run, the deviations being statistically relevant. The reason for the increasing productivity might be the increased hydrogenation of the catalyst coating with each run, due to the H_2 preconditioning procedure before each experiment, described in Section 2.4. The accumulating amount of H_2, which diffused into the layer, might have activated the catalyst even further and thus have led to an increased activity.

3.3.2. Corrosion and catalyst aging

As is generally known (e.g. [45]), the abrasion of coating layers decreases with exposure time until a virtually stationary state is reached. Weighing our samples before and after the test runs reveals that the decrease in catalyst mass lies below 3 % of the original catalyst mass. Repeated test runs showed an even further decrease in the measured mass loss. It can therefore also be assumed for our coatings that the observed catalyst mass loss stagnates after seven to 14 h on stream.

By optical inspection, minor losses and damaging of the coating can be detected, compare Fig. B.10 in the Appendix. Also, smaller traces of corrosion are found at the edges of the element. These areas are prone to corrosion, because of possible minor cracks in the coating, since the samples are mainly handled contacted in the edge areas to minimize shadowing during the coating and unwanted mechanical abrasion during the mounting process in the reactor.

ICP-OES measurements have been conducted to study the composition of the catalyst layers after the tests and to analyse possible corrosion residues stemming from the stainless steel carrier structure. The results show that no detectable Pd-loss was observed. The detailed analysis results can be found in the Appendix.

Taking into account the stability of the mean productivity of the coatings, the low mass loss and the ICP-OES results, it can be assumed that no significant deactivation of the catalyst layer is to be expected even with repeated use under operating conditions.

3.4. Reproducibility of the washcoating procedure

For possible later industrial applications, the reproducibility, and therefore reliability, of the coating procedure itself has to be ensured. Therefore, specimens of samples prepared with the same coating method

in this work are compared with each other regarding their productivity and the amount of deposited catalyst. Weighing of the catalyst carrier structures before and after the washcoating shows that the same amount of catalyst is deposited in each run (see Table 1).

Fig. 9a presents the measured productivity towards H_2O_2 over time of two sample specimen coated via the same washcoating procedure and with comparable H_2-exposure times. Since the mean productivity over 7 h on stream determined (see Fig. 9b) is comparable for the two repeat samples from different coating batches and the measured amounts of deposited catalyst are in good agreement within the different batches, it can be concluded that the washcoating process is robust and produces repeatable coatings with comparable catalytic activities.

4. Conclusion and outlook

Additively manufactured structured catalysts present a versatile solution for the replacement of suspended catalysts often used in the direct synthesis of H_2O_2. In this work we showed that our suggested coating mechanism for the application of a Pd/TiO_2 catalyst on steel surfaces via washcoating can produce catalytic layers that are stable, reproducible and active for the direct synthesis reaction.

Further investigations on materials characteristics such as active metal loading, catalyst treatment and catalyst particle size are required to continue to optimise the presented catalytically active coatings. Moreover, the coated substrates need to be tested in the envisioned membrane reactor design to test this concept for the decentralised production of H_2O_2.

CRediT authorship contribution statement

Laura L. Trinkies: Conceptualization, Methodology, Investigation, Data curation, Writing – original draft, Writing – review & editing, Visualization, Supervision, Project administration. **Derrick Ng:** Methodology, Resources, Writing – review & editing. **Zongli Xie:** Methodology, Resources, Writing – review & editing. **Christian H. Hornung:** Conceptualization, Methodology, Writing – review & editing, Supervision. **Manfred Kraut:** Methodology, Writing – review & editing, Supervision. **Roland Dittmeyer:** Writing – review & editing, Funding acquisition.

Declaration of Competing Interest

The authors declare that they have no known competing financial interests or personal relationships that could have appeared to influence the work reported in this paper.

Data availability

Data will be made available on request.

Appendix A. Sample overview

Table A2

Table A.2
Detailed overview of the investigated samples.

Identifier	Catalyst type	Support material	Pd-loading	Specimen identifier (optional)	No. of experiment (optional)
WC-10-5	washcoating	Al_2O_3	5 wt.-%	–	–
WC-01-5	washcoating	TiO_2	5 wt.-%	–	–
WC-01-1(-A/B-I/II/III)	washcoating	TiO_2	1 wt.-%	A,B	I, II, III
FB-01-1	fixed bed	TiO_2	1 wt.-%	–	–

Appendix B. Optical visible surface alterations

Fig. B10

(a)   (b)
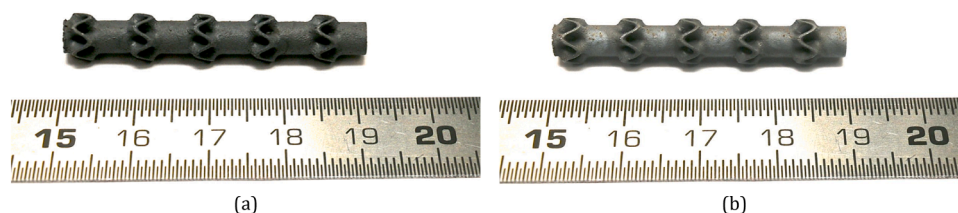
Fig. B.10. Pictures of a coated sample before (a) and after (b) seven hours on stream. Minor altered areas are clearly visible at the edges of the specimen after the exposure to reaction conditions.

Appendix C. ICP-OES results

Note: The given values are always relative to the analysed mass. Elements such as oxygen can not be determined by ICP-OES method. This explains the deviation of the sum of weight of the detected elements from the total sum. It is also important to notice that by a higher relative share of metals as chrome or nickel, stemming from the steel substrate, a lower relative share of titanium is to be expected. Recalculating the ratio of palladium to titanium, however, leads to stable palladium loading after the exposition to the reaction conditions.

Fig. 11C
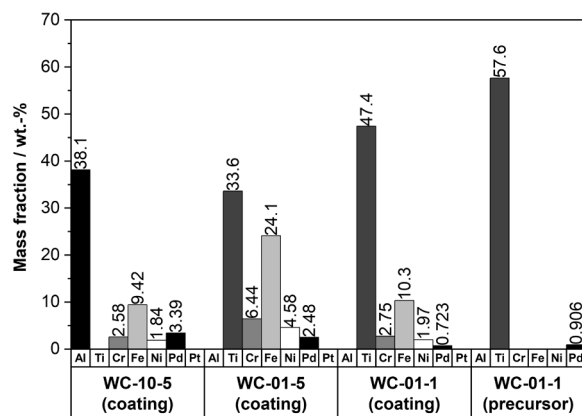
Fig. C.11. ICP-OES results: mass fraction of the measurable components of the coatings, scraped off after the experiments, and a fresh washcoating catalyst.

References

[1] R.J. Lewis, G.J. Hutchings, Recent advances in the direct synthesis of H_2O_2, ChemCatChem 11 (1) (2019) 298–308, https://doi.org/10.1002/cctc.201801435.

[2] Hydrogen peroxide market by end-user and geography - forecast and analysis 2022-2026, accessed: 04.07.2022 (2022). URL https://www.technavio.com/report/hydrogen-peroxidemarket-industry-analysis?utm_source=prnewswire&utm_medium=pressrelease&utm_campaign=&utm_content=IRTNTR70146.

[3] J.M. Campos-Martin, G. Blanco-Brieva, J.L.G. Fierro, Hydrogen peroxide synthesis: an outlook beyond the anthraquinone process, Angew. Chem. Int. Ed. Engl. 45 (42) (2006) 6962–6984, https://doi.org/10.1002/anie.200503779.

[4] R. Ciriminna, L. Albanese, F. Meneguzzo, M. Pagliaro, Hydrogen peroxide: a key chemical for today's sustainable development, ChemSusChem 9 (24) (2016) 3374–3381, https://doi.org/10.1002/cssc.201600895.

[5] D.W. Flaherty, Direct synthesis of H_2O_2 from H_2 and O_2 on pd catalysts: current understanding, outstanding questions, and research needs, ACS Catal. 8 (2) (2018) 1520–1527, https://doi.org/10.1021/acscatal.7b04107.

[6] G. McDonnell, The use of hydrogen peroxide for disinfection and sterilization applications, in: Z. Rappoport (Ed.), PATAI'S Chemistry of Functional Groups, John Wiley & Sons, Ltd, Chichester, UK, 2009, pp. 1–34, https://doi.org/10.1002/9780470682531.pat0885.

[7] G. Goor, J. Glenneberg, S. Jacobi, J. Dadabhoy, E. Candido, Hydrogen peroxide, in: Ullmann's Encyclopedia of Industrial Chemistry, WileyVCH Verlag GmbH & Co. KGaA, Weinheim, Germany, 2000, pp. 1–40, https://doi.org/10.1002/14356007.a13_443.pub3.

[8] C. Samanta, Direct synthesis of hydrogen peroxide from hydrogen and oxygen: an overview of recent developments in the process, Appl. Catal. A 350 (2) (2008) 133–149, https://doi.org/10.1016/j.apcata. 2008.07.043.

[9] Y. Yi, L. Wang, G. Li, H. Guo, A review on research progress in the direct synthesis of hydrogen peroxide from hydrogen and oxygen: noble-metal catalytic method, fuel-cell method and plasma method, Catal. Sci. Technol. 6 (6) (2016) 1593–1610, https://doi.org/10.1039/C5CY01567G.

[10] V. Paunovic, J.C. Schouten, T.A. Nijhuis, Direct synthesis of hydrogen peroxide in a wall-coated microchannel reactor over Au–Pd catalyst: a performance study, Catal. Today 248 (2015) 160–168, https://doi.org/10.1016/j.cattod.2014.04.007.

[11] S. Yang, A. Verdaguer-Casadevall, L. Arnarson, L. Silvioli, V. Čolić, R. Frydendal, J. Rossmeisl, I. Chorkendorff, I.E.L. Stephens, Toward the decentralized electrochemical production of H_2O_2: a focus on the catalysis, ACS Catal. 8 (5) (2018) 4064–4081, https://doi.org/10.1021/acscatal.8b00217.

[12] Deadly fire and explosions at container depot in Bangladesh: 48 dead and hundreds injured as hydrogen peroxide containers exploded, accessed: 23.06.2022 (2022). URL https://www.chemistryworld.com/news/deadly-fireand-explosions-at-container-depot-in-bangladesh/4015799.

[13] H. You, C. Fu, M. Wang, C. Yang, Y. Shi, H. Pan, Q. Lin, Pd/CNT with controllable Pd particle size and hydrophilicity for improved direct synthesis efficiency of H_2O_2, New J. Chem. (2022), https://doi.org/10.1039/D2NJ01638A.

[14] T. Richards, R.J. Lewis, D.J. Morgan, G.J. Hutchings, The direct synthesis of hydrogen peroxide over supported Pd-based catalysts: an investigation into the role of the support and secondary metal modifiers, Catal. Lett. (2022), https://doi.org/10.1007/s10562-022-03967-8.

[15] S. Shaybanizadeh, R. Luque, A. Najafi Chermahini, Facile synthesis of Pd–Au/BNNS bimetallic catalysts for direct generation of H_2O_2 from H_2 and O_2 under environmentally friendly conditions, Green Chem. (2022), https://doi.org/10.1039/D2GC00918H.

[16] Y. Shi, D. Jiang, J. Zhao, L. Wu, C. Zhao, J. Ma, H. Pan, Q. Lin, Synthesis and performance of Pd multi @HCS catalysts with Pd nanoparticles partially embedded in the inner wall of hollow carbon spheres for the direct synthesis of hydrogen peroxide from hydrogen and oxygen, New J. Chem. (2022), https://doi.org/10.1039/D2NJ01778D.

[17] T. Inoue, K. Ohtaki, S. Murakami, S. Matsumoto, Direct synthesis of hydrogen peroxide based on microreactor technology, Fuel Process. Technol. 108 (2013) 8–11, https://doi.org/10.1016/j.fuproc.2012.04.009.

[18] G. Vilé, D. Ng, Z. Xie, I. Martinez-Botella, J. Tsanaktsidis, C.H. Hornung, 3D–printed structured reactor with integrated single–atom catalyst film for hydrogenation, ChemCatChem (2022), https://doi.org/10.1002/cctc.202101941.

[19] M. Selinsek, M. Bohrer, B.K. V.ankayala, K. Haas-Santo, M. Kraut, R. Dittmeyer, Towards a new membrane micro reactor system for direct synthesis of hydrogen peroxide, Catal. Today 268 (2016) 85–94, https://doi.org/10.1016/j.cattod.2016.02.003.

[20] M. Selinsek, M. Kraut, R. Dittmeyer, Experimental evaluation of a membrane micro channel reactor for liquid phase direct synthesis of hydrogen peroxide in continuous flow using Nafion® membranes for safe utilization of undiluted reactants, Catalysts 8 (11) (2018) 556, https://doi.org/10.3390/catal8110556.

[21] F. Haber, R.Le Rossignol, Über die technische Darstellung von Ammoniak aus den Elementen, Z. Elektrochem. Angew. Phys. Chem. 19 (2) (1913) 53–72, https://doi.org/10.1002/bbpc.19130190201.

[22] M. Baumann, T.S. Moody, M. Smyth, S. Wharry, A perspective on continuous flow chemistry in the pharmaceutical industry, Org. Process Res. Dev. 24 (10) (2020) 1802–1813, https://doi.org/10.1021/acs.oprd.9b00524.

[23] F. Kapteijn, J.A. Moulijn, Structured catalysts and reactors – perspectives for demanding applications, Catal. Today 383 (2022) 5–14, https://doi.org/10.1016/j.cattod.2020.09.026.

[24] A. Avril, C.H. Hornung, A. Urban, D. Fraser, M. Horne, J.-.P. Veder, J. Tsanaktsidis, T. Rodopoulos, C. Henry, D.R. G.unasegaram, Continuous flow hydrogenations using novel catalytic static mixers inside a tubular reactor, React. Chem. Eng. 2 (2) (2017) 180–188, https://doi.org/10.1039/C6RE00188B.

[25] M. Kundra, T. Grall, D. Ng, Z. Xie, C.H. Hornung, Continuous flow hydrogenation of flavorings and fragrances using 3D-printed catalytic static mixers, Ind. Eng. Chem. Res. (2021), https://doi.org/10.1021/acs.iecr.0c05671.

[26] Y. Zhu, B. Bin Mohamad Sultan, X. Nguyen, C. Hornung, Performance study and comparison between catalytic static mixer and packed bed in heterogeneous hydrogenation of vinyl acetate, J. Flow Chem. (2021), https://doi.org/10.1007/s41981-021-00152-7.

[27] E. Hansjosten, A. Wenka, A. Hensel, W. Benzinger, M. Klumpp, R. Dittmeyer, Custom-designed 3D-printed metallic fluid guiding elements for enhanced heat transfer at low pressure drop, Chem. Eng. Process. - Process Intensif. 130 (May) (2018) 119–126, https://doi.org/10.1016/j.cep.2018.05.022.

[28] L.L. Trinkies, B.J. Deschner, E. Hansjosten, M. Kraut, R. Dittmeyer, 3D–printed fluid–guiding elements for flow control in a microstructured membrane reactor for H_2O_2 direct synthesis, Chem. Ing. Tech. 92 (9) (2020) 1364, https://doi.org/10.1002/cite.202055312.

[29] L.L. Trinkies, A. Düll, B.J. Deschner, A. Stroh, M. Kraut, R. Dittmeyer, Simulation of fluid flow during direct synthesis of H_2O_2 in a microstructured membrane reactor, Chem. Ing. Tech. 93 (5) (2021) 789–795, https://doi.org/10.1002/cite.202000232.

[30] R.B. Rankin, J. Greeley, Trends in selective hydrogen peroxide production on transition metal surfaces from first principles, ACS Catal. 2 (12) (2012) 2664–2672, https://doi.org/10.1021/cs3003337.

[31] L.C. Almeida, F.J. Echave, O. Sanz, M.A. Centeno, J.A. Odriozola, M. Montes, Washcoating of metallic monoliths and microchannel reactors, in: Scientific Bases for the Preparation of Heterogeneous Catalysts - Proceedings of the 10th International Symposium, Louvain-la-Neuve, Belgium, July 11-15, 2010 175, Elsevier, 2010, pp. 25–33, https://doi.org/10.1016/S01672991(10)75004-7.

[32] M. Selinsek, B.J. Deschner, D.E. Doronkin, T.L. Sheppard, J.-.D. Grunwaldt, R. Dittmeyer, Revealing the structure and mechanism of palladium during direct synthesis of hydrogen peroxide in continuous flow using operando spectroscopy, ACS Catal. 8 (3) (2018) 2546–2557, https://doi.org/10.1021/acscatal.7b03514.

[33] S.J. Freakley, Q. He, J.H. Harrhy, L. Lu, D.A. Crole, D.J. Morgan, E.N. Ntainjua, J. K. Edwards, A.F. Carley, A.Y. Borisevich, C.J. Kiely, G.J. Hutchings, Palladium-tin catalysts for the direct synthesis of H_2O_2 with high selectivity, Science 351 (6276) (2016) 965–968, https://doi.org/10.1126/science.aad5705.

[34] P. Kant, L.L. Trinkies, N. Gensior, D. Fischer, M. Rubin, G. Alan Ozin, R. Dittmeyer, Isophotonic reactor for the precise determination of quantum yields in gas, liquid, and multi-phase photoreactions, Chem. Eng. J. 452 (2023), 139204, https://doi.org/10.1016/j.cej.2022.139204.

[35] H_2O_2 Passivation Procedure. accessed: 25.03.2022 (2005). URL https://www.solvay.us/en/binaries/HH-056_Passivation236794.pdf.

[36] B.J. Deschner, D.E. Doronkin, T.L. Sheppard, G. Rabsch, J.-.D. Grunwaldt, R. Dittmeyer, Continuous-flow reactor setup for operando x-ray absorption spectroscopy of high pressure heterogeneous liquid-solid catalytic processes, Rev. Sci. Instrum. 92 (12) (2021), 124101, https://doi.org/10.1063/5.0057011.

[37] A. Pashkova, K. Svajda, R. Dittmeyer, Direct synthesis of hydrogen peroxide in a catalytic membrane contactor, Chem. Eng. J. 139 (1) (2008) 165–171, https://doi.org/10.1016/j.cej.2007.09.003.

[38] A. Pashkova, K. Svajda, G. Black, R. Dittmeyer, Automated system for spectrophotometric detection of liquid phase hydrogen peroxide for concentrations up to 5% w/w, Rev. Sci. Instrum. 80 (5) (2009), 055104, https://doi.org/10.1063/1.3120523.

[39] J. Brehm, R.J. Lewis, D.J. Morgan, T.E. Davies, G.J. Hutchings, The direct synthesis of hydrogen peroxide over AuPd nanoparticles: an investigation into metal loading, Catal. Lett. 152 (1) (2022) 254–262, https://doi.org/10.1007/s10562-021-03632-6.

[40] N. Gemo, S. Sterchele, P. Biasi, P. Centomo, P. Canu, M. Zecca, A. Shchukarev, K. Kordás, T.O. S.almi, J.-.P. Mikkola, The influence of catalyst amount and Pd loading on the H_2O_2 synthesis from hydrogen and oxygen, Catal. Sci. Technol. 5 (7) (2015) 3545–3555, https://doi.org/10.1039/C5CY00493D.

[41] L. Fu, S. Liu, Y. Deng, H. He, S. Yuan, L. Ouyang, Fabrication of the PdAu surface alloy on an ordered intermetallic Au_3Cu core for direct H_2O_2 synthesis at ambient pressure, Ind. Eng. Chem. Res. 61 (32) (2022) 11655–11665, https://doi.org/10.1021/acs.iecr.2c01482.

[42] T. Deguchi, M. Iwamoto, Catalytic properties of surface sites on Pd clusters for direct H_2O_2 synthesis from H_2 and O_2: a DFT study, J. Phys. Chem. C 117 (36) (2013) 18540–18548, https://doi.org/10.1021/jp4056297.

[43] Z. Panossian, N.L. de Almeida, R.M.F. de Sousa, G. d. S. Pimenta, L.B.S. Marques, Corrosion of carbon steel pipes and tanks by concentrated sulfuric acid: a review, Corros. Sci. 58 (2012) 1–11, https://doi.org/10.1016/j.corsci.2012.01.025.

[44] T. Satoh, S. Uchida, J.-i. Sugama, N. Yamashiro, T. Hirose, Y. Morishima, Y. Satoh, K. Iinuma, Effects of hydrogen peroxide on corrosion of stainless steel, (I): improved control of hydrogen peroxide remaining in a high temperature high pressure hydrogen peroxide loop, J. Nucl. Sci. Technol. 41 (5) (2004) 610–618, https://doi.org/10.1080/18811248.2004.9715524.

[45] M. Adamowska, P.Da Costa, Structured Pd/γ-Al_2O_3 prepared by washcoated deposition on a ceramic honeycomb for compressed natural gas applications, J. Nanoparticles (2015) 1–9, https://doi.org/10.1155/2015/601941.